VĚDECKÉ SPISY VYSOKÉHO UČENÍ TECHNICKÉHO V BRNĚ

Edice PhD Thesis, sv. 869

ISSN 1213-4198

Ing. Marek Zbončák

Magnetically Assembled Nanoparticle Structures and their Effect on Mechanical Response of Polymer Nanocomposites

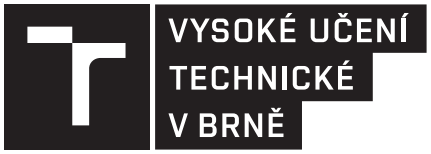

CENTRAL EUROPEAN INSTITUTE OF TECHNOLOGY

STŘEDOEVROPSKÝ TECHNOLOGICKÝ INSTITUT

MAGNETICALLY ASSEMBLED NANOPARTICLE STRUCTURES AND THEIR EFFECT ON MECHANICAL RESPONSE OF POLYMER NANOCOMPOSITES

MAGNETICKY USPOŘÁDANÉ STRUKTURY V POLYMERNÍCH NANOKOMPOZITECH A JEJICH VLIV NA MECHANICKOU ODEZVU

ZKRÁCENÁ VERZE PH.D. THESIS

OBOR	Pokročilé materiály
AUTOR PRÁCE	Ing. Marek Zbončák
ŠKOLITEL	prof. RNDr. Josef Jančář, CSc.
OPONENTI	doc. Ing. Viera Khunová, Ph.D. prof. Alfred J. Crosby
DATUM OBHAJOBY	11. prosince 2018

Brno 2018

Keywords:

Polymer nanocomposites, Self-assembly, Magnetic directed self-assembly, Bottom-up assembly, Aggregation, Magnetic interaction, Thermo-mechanical properties, Anisotropy, Multi-level hierarchy, Polymer immobilization, Structure-property relationships

Klíčová slova:

Polymerní nanokompozity, Samo-uspořádávání, Magneticky řízené samouspořádávání, Bottom-up uspořádávání, Agregace, Magnetická interakce, Termo-mechanické vlastností, Anisotropie, Více úrovňová hierarchie, Imobilizace polymeru, Vztah mezi strukturou a vlastnostmi

Místo uložení originálu dizertační práce:

Vysoké učení technické v Brně
Středoevropský technologický institut
Purkyňova 123
Brno 612 00
Česká Republika

ISBN 978-80-214-5704-1
ISSN 1213-4198

List of Contents

1 INTRODUCTION

1.1 Magnetically directed self-assembly in polymer composites

Despite relentless attempts of researchers to achieve a control over the assembling of the nanoparticles (NPs) in polymer matrix, common isotropic particle assemblies are typical output of their efforts – dispersion, clusters, aggregates[1, 2]. Compared to self-assembly techniques which are most commonly employed for preparation of polymer nanocomposites (PNCs), magnetic directed self-assembly can produce various anisotropic structures with a conveniently controlled and homogenous orientation. Therefore, it is not surprise that this technique found its place among the processing protocols for PNCs. Individual MNP represent a magnetic dipole consisted from the north and south pole and adjacent magnetic dipoles interact with each other via their magnetic fields and assemble into complex anisotropic structures[3]. The resulted structure depends on multiple processing parameters such as strength, shape and gradient of magnetic field, particle concentration and inter particle distance, magnetic response of the particles, viscosity of environment or assembling time[4-14]. For the fabrication of magnetically assembled PNCs, various laboratory scale processing techniques have been used by researchers. Methods such as solution casting of thin polymer films[15-19], bulk *in-situ* thermal[20-30] or photo[31-33] polymerization during magnetic irradiation of the samples are most frequently used.

1.2 Thermo-mechanical properties of polymer nanocomposites

Addition of NPs into polymer matrix results in non-trivial enhancement of macroscopic thermo-mechanical response. Classic composite micromechanics theories which are quite viable to explain the mechanical response of micro composites fail in the case of polymer nanocomposites[34, 35]. When loading of NPs in polymer matrix remains low, commonly very modest enhancement of PNC's modulus is observed bellow T_g. However, vast enhancement of PNC's modulus is observed around and above the glass transition. In the field of PNCs, two reinforcing mechanisms are respected among the researchers: *i*) altered relaxations of polymer segments via their interactions with nanoparticle[36-44] and *ii*) sort of stress-transfer via interconnected particle superstructures[43-54].

The mechanical properties of magnetically assembled nanoparticle structures were studied by various authors using different polymer matrices filled with micro[22], sub-micro[21] or nano sized magnetic particles[15, 17, 55, 56]. Increased modulus of the composites with longitudinally oriented particle structures is exhibited while significant mechanical anisotropy is observed when longitudinally, transversely and/or randomly oriented structures are compared. However, reinforcing mechanisms rather left unanswered. Mechanical properties were usually investigated in close proximity or far above of T_g of the polymer matrix.

2 AIM OF THESIS

Impulse of external magnetic field initiates controlled assembling process of magnetic nanoparticles into ordered nano and microstrucutres. Magnetic dipole interactions are driving force of this process and dependent on the strength of external magnetic field, while environmental resistance of polymer matrix counteracts against these forces. Also, initial particle packing has a large impact on the balance of magnetic forces between particles and determines the size and structure of primary assembling blocks. The aim is to evaluate the influence of these processing parameters on the resulted structure with a respect to the kinetics of this process. Structural parameters will be used for interpretation of mechanical properties of these nanocomposites.

3 MATERIALS AND METHODS

3.1 Sample preparation

Photocurable resin was composed from poly(ethylene glycol) dimethacrylate (PEGDMA) (99 %, Sigma-Aldrich, USA), with a molecular weight of PEG part, $M_{n(PEG)}$=750 g·mol^{-1} and total molecular weight of monomer molecule is M_r=904.0 g·mol^{-1}; and ethoxylated bisphenol A dimethacrylate monomer (bis-EMA) (>87%, Esschem Europe, United Kingdom). Monomers were mixed in the molar ratio 22/78 and 1 molar % (0.75 wt. %) of phenylbis(2,4,6-trimethylbenzoyl)phosphine oxide (BAPO) (97%, Sigma-Aldrich, USA) was added into the mixture of the monomers as a photo initiator.

The synthesized magnetite nanoparticles were used as a magnetic filler in photocurable polymers and colloids. Particle exhibits spherical morphology and log-normal distribution of diameters with mean diameter, d=16 nm. The weight of particles corresponding to 1 or 2 vol. % was added into 40 ml of the photopolymer resin and subjected to continuous ultrasound dispersion with ultrasound homogenizer Sonoplus HD 3200 (Bandelin, Germany) while rapid cooling of suspension.

Small volume of the particle suspension was drop casted between two quartz glass microscopy slides covered with a thin cellophane foil. The mould was placed on quartz glass platform in the center of the solenoid. Magnetic field (B=0, 5, 25, 50 mT) was applied for entire time of the sample preparation. After certain time of magnetic irradiation (t_a=0, 5, 10, 20, 30, 60, 300 sec) for the particle assembly, UV light generated by the light source OmniCure S2000 (Excelitas Technologies, USA) was applied. After photopolymerization, thin film samples were demoulded and post cured in a vacuum oven at 100 °C for 1 hour under vacuum.

3.2 Structural analysis

The morphology and size of particles, structure of the nanocomposites and particle assemblies was investigated by the scanning electron microscope (SEM) Mira3 XM (TESCAN, Czech Republic) in secondary electrons (SE), back-scattered electrons (BSE) and/or in transmission mode (STEM). Samples for SEM were polished using TEM Mill 1050 (Fischione Instruments, USA) and very thin layer of the sample surface was milled off for the structures to be observable by the electron microscopy. Thin slices for STEM and HR-TEM were prepared by Ultramictome EM UC7 (Leica Microsystems, Germany).

3.3 Dynamic mechanical analysis

Dynamic mechanical analyzer for the solid samples RSA G2 (TA Instruments, USA) was used for the measurements of thermo-mechanical properties of the samples in tension with an axial deformation of ε=0.05 %, frequency f=1 Hz and top-down temperature ramp from 170 °C to -100 °C with a cooling rate 5 °C/min.

3.4 Magnetic properties

Magnetic properties of synthesized magnetic nanoparticles were measured with a use of Mini Cryogen-Free Magnet System (Cryogenic Limited, United Kingdom) at the laboratory temperature T=298 K (temperature of assembling).

4 RESULTS AND DISCUSSION

4.1 Structure

4.1.1 Self-assembly aggregation, B=0 mT

Initial self-assembled structures exhibit relatively extensive aggregation of MNPs into sub-micron irregularly shaped assemblies with small aggregates (quasi isotropic, composed from few particles) homogenously distributed in the sample volume (Figure 1). Lower particle loading, 1 vol. %, exhibits rather isolated particle aggregates (Figure 1A) in contrary to 2 vol. % sample with considerably bigger and microscopically percolated particle structures (Figure 1B). The adsorption of low molecular weight photopolymer monomers such as those used in the experiments apparently cannot sufficiently stabilize the particle dispersion by the steric repulsion despite the presence of numerous polar bonds in PEG chains and ester bonds (~CO–O–CH_2–CH_2–O~). It will be later shown that close MNPs are spaced with a thin layer of polymer and structures are something between aggregate and cluster. Despite various stabilizing strategies, problematic dispersion and spontaneous aggregation of MNPs in photopolymer matrix[33, 57, 58], other polymer solutions and melts[16, 59-64] has been reported also previously by numerous researchers.

It was proposed that aggregation of MNPs in liquid polymer matrix undergoes two steps aggregation process[15, 61]. In the first step, primary aggregates composed from few of particles (for example 10) are created via interparticle interactions such as van der Waals, or electrostatic (including the magnetic attraction is highly reasonable). In the second step, primary aggregates form the secondary fractal aggregates as a volume fraction of MNPs increases above ϕ>0.01 vol. %. Few isolated, most probably kinetically entrapped, self-assembled structures consisted from several particles with a diameter ~50-100 nm and little bit larger ~150 nm for ϕ=1 and 2 vol. %, respectively were found within the polymer matrix. Small number of even smaller (few particle) aggregates and single particles were found during the analysis of multiple STEM images at high magnifications, but the presence of these objects is rather exceptional and rare. Despite the origin of the primary aggregates (dispersion of powder vs. self-assembly aggregation) is uncertain, these small objects are building blocks for any other structures which further grow in the system with or without the external magnetic field. They either exist in the colloid suspension from the beginning or they are formed very quickly. Fractal-like aggregates in this work such as those in Figure 1 were created by a complex multi-step aggregation of smaller particle structures (primary aggregates) into large fractal aggregates with an irregular. Two populations of primary aggregates of different

shape and size were observed. The isotropic spherical and anisotropic aggregates with elliptical shape a slightly larger number of particles and volume.

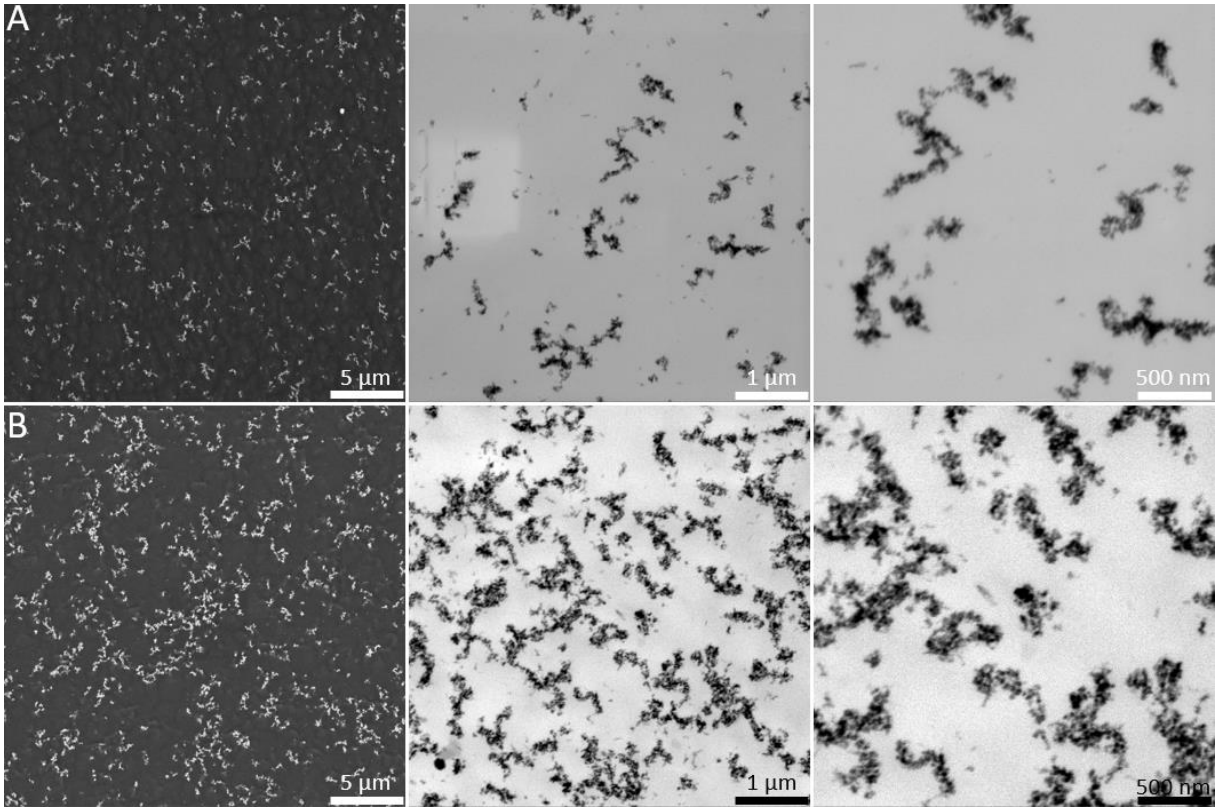

Figure 1 Electron microscopy images of the particle structure in the photopolymer matrix at filler loading (A) ϕ=1 vol. % and (B) ϕ=2 vol. % in absence of the external magnetic field, B=0 mT. BSE and STEM modes, low, medium and high magnifications.

Remanent magnetization measured at the zero field accompanied by the particle aggregation was experimentally observed by Robbes et al.[61] or Bharti et al.[65], however, effect of the magnetic interactions on the aggregation process was not studied. To address the relative strength of van der Waals and magnetic interactions on the aggregation process, corresponding energetic potentials were calculated and normalized to thermal energy. Mean interparticle surface-to-surface distance[35] and mean shortest interparticle surface-to-surface distance[41] for randomly packed spheres is used assuming homogeneous initial dispersion of MNPs at filler loading ϕ=1 and 2 vol. %. (see Figure 2A).

Calculations of van der Waals[60] and magnetic[65-68] energies shows that magnetic interactions contribute to aggregation significantly on much longer ranges when compared to van der Waals attraction and contributes to aggregation process of two 16 nm magnetite particles up to interparticle distance Δl=20 nm at which equal to thermal energy (λ=1). Magnetic energy for mean shortest interparticle distances satisfactorily falls to the aggregation region (λ>1) while energetic values for mean interparticle distance remain still in diffusion region (λ<1). Interparticle distances exhibit much broader distribution of interparticle distances and consequently also much shorter distances than reported mean values exist in the system[69, 70].

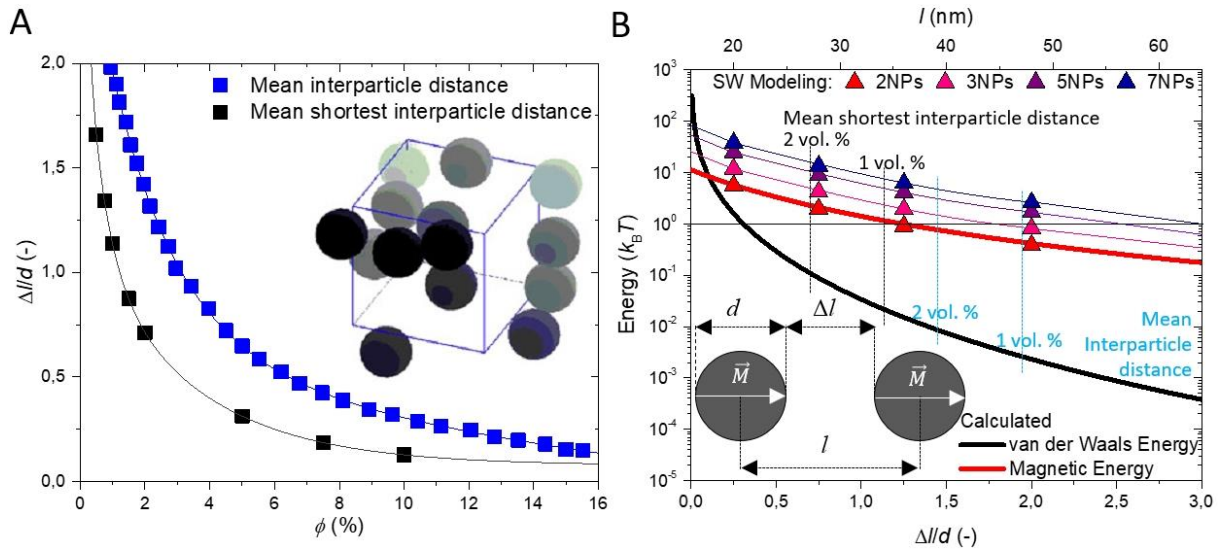

Figure 2 (A) Mean interparticle distance normalized to the particle diameter as a function of filler volume fraction, data acquired from ref.[35, 41]. Inset shows structure of PNC with a random particle packing. Reprinted from ref.[35], Copyright 2010, with permission from Elsevier. (B) Calculated van der Waals (solid black line) and magnetic interaction energy (solid red line) between two MNPs, d=16 nm as a function of their interparticle distance in the units of thermal energy (k_BT). Inset depicts the particle arrangement. Triangles represent micromagnetic simulations of mutual magnetic interaction energy for increasing number of in-line aligned MNPs: 2–red, 3–pink, 5–purple and 7 MNPs – blue.

4.1.2 Magnetically assembled structures

The application of magnetic field triggered rapid assembling of magnetic building blocks into anisotropic chain-like assemblies with a homogeneous orientation controlled by the external magnetic field. In the magnetic field, particles rapidly form various types of structures and their mutual interactions are enhanced as magnetic moments are more aligned in direction of the field when compared to zero field sample. Magnetic building blocks create stronger local magnetic field resulting from the contribution of external field and magnetization of particles aggregates. Higher extent of alignment, longer and larger structures are assembled under higher external magnetic fields as can be seen in Figure 3. The anisotropic structures are perfectly oriented in the field direction. One-dimensional structures are gradually merged in longitudinal and lateral direction and create superstructures under intense external fields, higher particle loading or extended assembling times.

Assembling in low magnetic field,* B=*5 mT

At a low particle concentration, ϕ=1 vol. %, magnetic structures are elongated along the field direction and assembled into superstructures guided by the low magnetic field, B=5 mT. These superstructures are formed from the individual aggregates interconnected by head to tail magnetic interactions acting between them (Figure 3). These superstructures are homogenously oriented along the field direction. Two processes proceed simultaneously in this system with a low magnetic

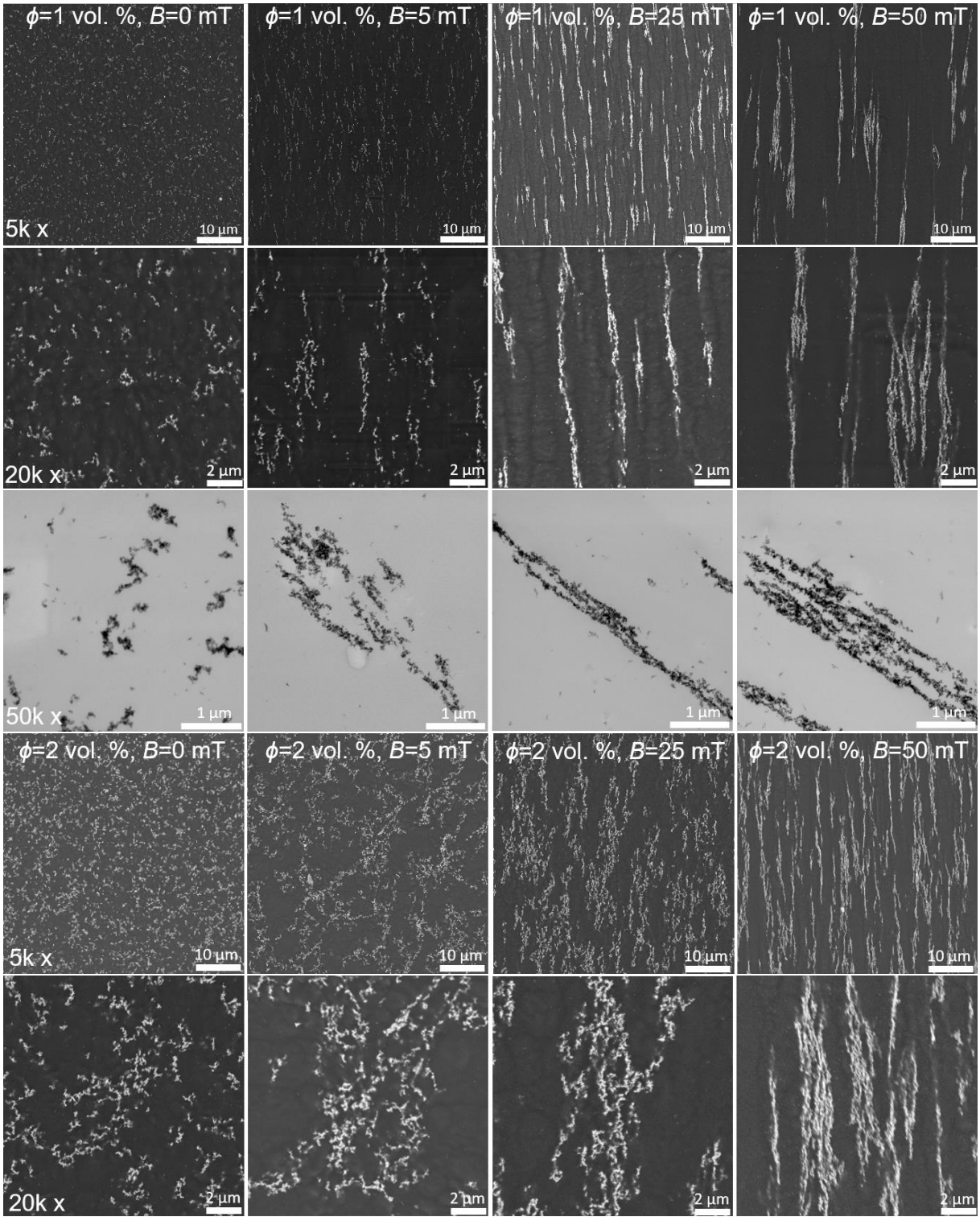

Figure 3 SEM and STEM images of self-assembled structure in absence of external magnetic field and magnetically directed self-assembled structures in presence of external magnetic fields B=5, 25 and 50 mT at particle loading ϕ=1 and 2 vol. %, after t_a=10 sec. Images at low, intermediate magnification in BSE mode and high magnification in STEM mode.

field: *i*) self-assembly aggregation of MNPs and *ii*) their magnetic alignment. Low external magnetic field, B=5 mT, rather results in the concentration, straightening and chaining of adjacent (self-assembled) neighboring aggregates into large

superstructures along the imaginary force lines of the magnetic field while self-assembly process has a major effect on the growth of individual aggregates. Increased loading of MNPs, ϕ=2 vol. %, shows transition from the anisotropic sub-micro aggregates to microscopically percolated assemblies (Figure 3) with no preferential alignment or anisotropy which is further developed after the extended assembling times. These microscopic flocculates are created by the drag and concentration of the magnetic material in one spot and thus large particle-free domains are formed.

Assembling in higher magnetic fields,* B=*25 mT and* B=*50 mT

Increase of magnetic field to *B*=25 mT and 50 mT led to more rapid organization of MNPs into well-developed anisotropic structures with a high aspect ratio (in the system containing ϕ=1 vol. %). Magnetic material is concentrated along the imaginary force lines of the field. Again, structures are homogenously oriented with a long axis of the magnetic chain backbone aligned along the direction of the applied magnetic field. From both SEM and STEM images (Figure 3), it is clearly seen that these superstructures are built from individual particle chains that are several particles wide and micrometres long. These one-dimensional structures interact with each other by head-to-tail magnetic interactions creating longitudinally interconnected superstructures. The widening of the structures is caused by an instability of repulsive interchain magnetic interactions which results in their lateral merging and formation of chain junctions. This is especially visible for the strongest magnetic field, *B*=50 mT. Large magnetic structures are surrounded by stronger magnetic field while smaller assemblies have a higher mobility in viscous matrix. Growing structures gradually attract and absorb smaller magnetic building blocks from 3D area around them during the magnetic directed self-assembly and increase their volume[24, 65].

The diameter of the magnetic chains is very close to diameter of primary aggregates found in nanocomposites. With a diameter ~100 nm, aspect ratio (*L*/*D*) of the structures easily exceeds the values ~100. However, mean values of chain's aspect ratio lie around ~25-29 due to presence of shorter structures (see Figure 3 for *B*=25 and 50 mT in low magnification). This is more evident and frequent for the structure assembled under *B*=50 mT. The length of some particles assemblies considerably exceeds the length of those assembled under *B*=25 mT but lot of relatively short and thick particle chains are found in the system as well, which consequently decrease mean length/aspect ratio when compared to system assembled under *B*=25 mT. As well, these structures show higher extent of lateral merging but they still remain mainly individual with a spacing polymer between them. Additional lateral merging of the structures is more obvious after extended assembling time or increased concentrations of MNPs (discussed further in text). The assembling of the individual particle chains into one dimensional particle superstructures is a perfect example of complex bottom-up built-up approach.

4.2 Thermo-mechanical properties

The mechanical anisotropy of magnetically assembled nanoparticle systems was studied by various authors[15, 17, 21, 22, 55, 71-74]. Despite research done in this field, reinforcing mechanisms of anisotropic chain-like particle structures are not fully understood yet.

4.2.1 Glass transition

Glass transition of neat polymer matrix (PEGMA/bis-EMA=22/78) was evaluated as T_g=45.1±3.9 °C. Its position shifts to lower temperatures and decreases by more than ΔT_g>-5 °C with an addition of 1 vol. % of magnetic nanoparticles which are aggregated into complex sub-micro structures. This decrease is caused by the absorption of the light during the photocuring by magnetite nanoparticles and especially by their larger aggregates/structures[33, 57]. Particle structures work as efficient light absorbers/scattering objects for the light despite their diameter is bellow critical dimension which equals to wave length absorbed by the photoinitiator (λ=370-400 nm)[75]. For larger structures than this length, penetration of light is almost impossible. Light required for initiation and cleavage of photoinitiator thus may not penetrate properly the depth of the sample which is even pronounced for growing structures in magnetic field. With an increase of interchain distance occurring at B=25 and 50 mT, light penetrates trough the magnetite free domains – optical paths of neat matrix and T_g starts to upturn[33]. In addition, light has limited possibility to penetrate inner structure of particle assemblies and cross-link the monomers entrapped here. Later, it will be shown that this polymer fraction is essential for thermo-mechanical properties of PNCs. Thermal post curing generates additional initiating radicals and repeatably trigger the cross-linking radical polymerization, however mobility of free radicals is slower and limited by the diffusivity of free radicals trough the polymer network although temperature is far above T_g.

The presence of the immobilized layer of polymer on the NPs is assessed by various analytical methods[76] but the most commonly, the increase of T_g of composite is the most straight forward evidence of altered relaxations. Due to decrease of cross-linking density with an addition of MNPs and their structuring by magnetic interactions, T_g of PNCs is gradually decreasing[77], hence the presence of polymer chains with retarded dynamics cannot be qualitatively and directly evidenced by analysis of T_g. On the other hand, this does not mean that polymer chains are not immobilised/confined by particle surface. The polymer network in the presence of MNPs just has a smaller cross-linking density than the unfilled matrix. Repulsive NP-polymer interaction is not expected.

4.2.2 Mechanical properties in glassy region

The complete temperatures spectrum (from -100 °C to 170 °C) of the storage moduli of the magnetic PNCs is shown in Figure 4A,B for both longitudinal and transverse direction, respectively. Insignificant effect of the particles and their

assemblies on the mechanical response is observed bellow glass transition of the system while substantial difference in modulus is observed above glass transition. Storage modulus is normalized to modulus of neat polymer matrix for both regions – glassy and rubbery and shown in graph in Figure 4C.

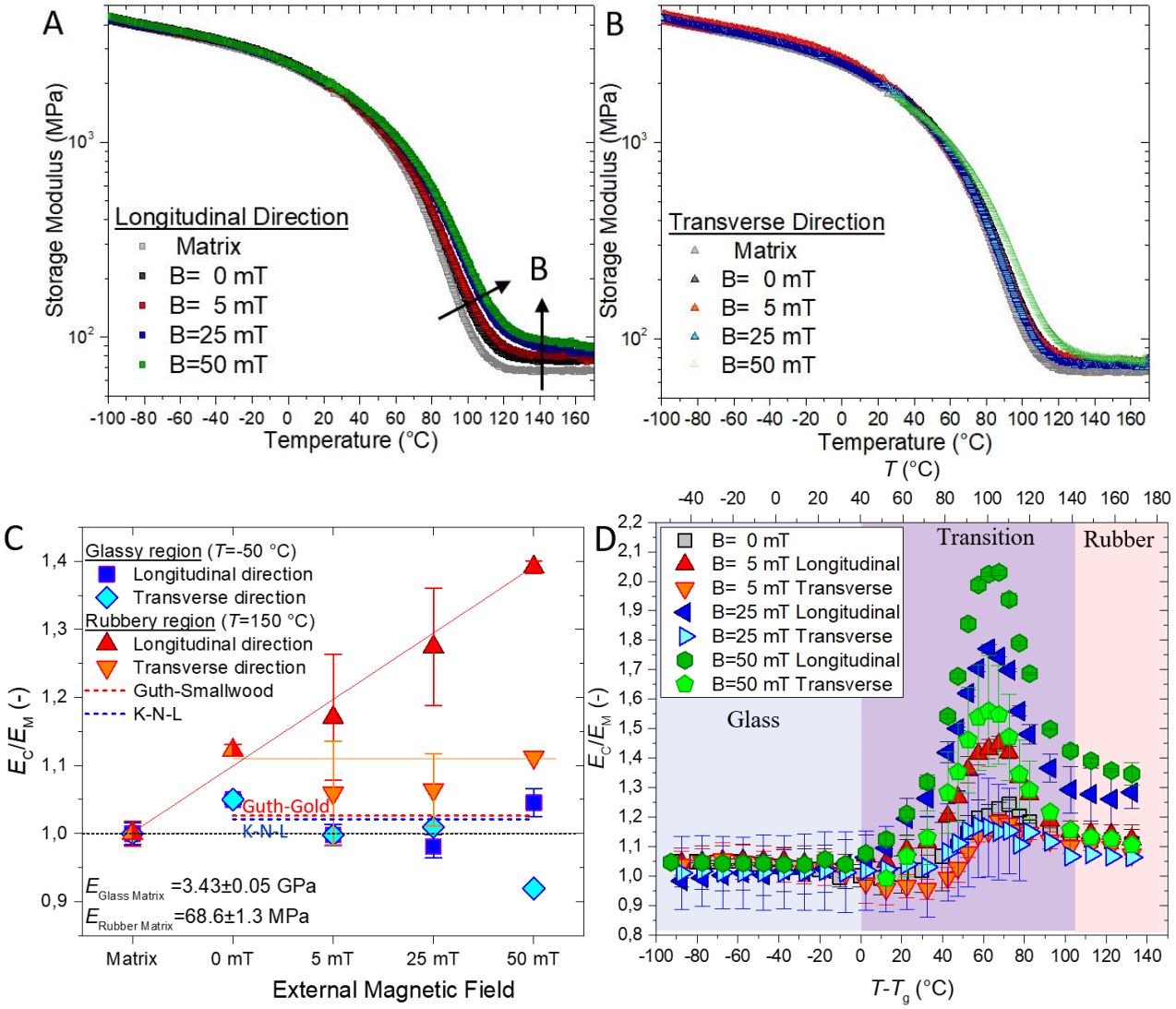

Figure 4 DMA temperature ramp spectrum for photopolymer matrix and its nanocomposites filled with ϕ=1 vol. % of Fe_3O_4 and assembled under magnetic fields B=0, 5, 25, 50 mT after t_a=10 sec. Storage modulus of PNCs films in (A) longitudinal and (B) transverse direction with a respect to the structure orientation as a function of temperature. (C) Storage modulus of composites normalized to modulus of neat matrix (E_C/E_M) as a function of the external magnetic field. (D) Relative composite modulus (E_C/E_M) for PNCs containing ϕ=1 vol. % of MNPs as a function of distance from T_g (T-T_g). Individual temperature relaxation time regions are marked as follows: glass – blue, transition – purple and rubber – red.

Mechanical properties of composites in glassy region scatter around boundary E/E_M=1 regardless of structure size or its orientation (Figure 4C). Negligible effect of NPs on the stiffness of PNCs in the glassy region is commonly known for decades. In this region, mechanical response of PNCs obeys a micro-mechanical

reinforcement given by the volume replacement mechanism – replacement of polymer with a stiffer phase (particles). This model accounts with a contribution of particle deformation to overall macroscopic deformation of PNC. And thus, it might be said that addition of fraction of 1 vol. % will have only marginal effect on the mechanical robustness of PNCs. Usually, higher volume fractions (or substantial modification of polymer matrix via particle-polymer interactions) are required to induce reinforcement of the glassy matrix. Experimental data of the storage modulus were fitted with a micro-mechanical Kerner-Nielsen-Lewis model which is commonly utilized for the particle filled polymers filled either with MPs or NPs [78]. This model predicts a stiffness of PNCs filled with ϕ=1 vol. % of MNPs as E_{KNL}=3.5 GPa which corresponds to normalized value E_{KNL}/E_M=1.021 (Figure 4C – blue dotted line). Data of glassy state modulus scatter around this trend line what means that reinforcing mechanisms can be explained by the volume replacement of softer polymer glass with much stiffer magnetic nanoparticles.

4.2.3 Mechanical properties in rubbery region

Rubbery modulus of neat matrix drops down by two orders of magnitude from glassy state with a stiffness E_M^G=3.43GPa to E_M^0=68.6 in rubbery plateau. In contrary to glassy region, large enhancement of composite stiffness and strong anisotropy was measured for the mechanical properties of PNCs far above their T_g. Relative values of the composite stiffness normalized to neat polymer modulus are plotted in Figure 4C. Difference between mechanical properties of polymer matrix and its PNCs starts to appear in proximity of the T_g of the polymer matrix. Course of storage modulus as well of tan δ starts to separate around T=20 °C and their different course becomes significant with an increasing temperature as soon as T_g is exceeded. For transversely oriented structures, almost constant enhancement of the rubbery modulus was measured comparable with a modulus of the self-assembled composites (Figure 4B,C). As well, tan δ shows same position and height of tan δ peak. Much stronger effect of the particles structures on the increase of the rubbery modulus is observed for their longitudinal orientation (Figure 4A,C) and modulus increases steadily with an increasing assembling field (with a growth of the particle structures in the sample).

Guth-Gold model[40, 79-81] is used for description on the mechanical properties of PNCs above T_g. In the photopolymer system, this model predicts a normalized rubbery modulus of nanocomposite as E^0_{GG}/E^0_M=1.026 (Figure 4C – red dotted line). Experimental data for both, longitudinal and transverse orientation in rubbery state show considerably higher values than a model prediction. Discrepancies between model and real experimental results are the most commonly debated on the background of the immobilized layer[40] or contribution form particle structure [81] concepts. The both theories seem to have their own logic and their mutual existence might be also explanation despite hardy to distinguish their individual contributions.

4.2.4 Mechanical properties in transition region

Relative values of PNC's modulus were plotted as a function of distance from the PNC's T_g (Figure 4D) to address the influence of the particle assemblies on the stiffness of PNCs in whole temperature range – glassy, transition and rubbery region. The effects in glassy and rubbery regions were already discussed in previous sections. Note that T_g of individual composites were used for the calculation of temperature distance (T-T_g). Large peak of relative composite stiffness can be observed in transition region exhibiting temperature dependent and viscoelastic reinforcement. Maximum is temperature independent for all samples regardless of structure size of its orientation. Note that self-assembled and magnetically assembled structures (B=0, 5, 25 mT) with a transverse orientation shows almost identical course of reinforcing effectivity.

4.2.5 Reinforcing mechanism

The modification of PNCs mechanical response is often attributed to adsorption of polymer chains on the surface of solid inclusions leading to creation of bound layer with altered relaxations[82, 83]. The thickness of bound layer is usually reported in the order of several nanometres (1-2 nm) depending on various chain properties and interactional strength[82, 84-87]. For example, Xu et al.[88] studied the adsorption of low molecular weight polypropylene glycol (PPG) on the silica NPs structured in continuous network and its contribution to viscoelastic and thermal response of PNCs. Anderson, Kim and Zukoski[89, 90] reported an adsorption of polyethylene glycol (PEG) with various molecular weights on the surface of silica NPs. Both teams reported bound polymer layer with a thickness in order of several nanometres for studied glycol molecules. Also, methacrylate esters are frequently reported to be successfully anchoring moiety in the presence of NPs[40-42, 44, 91].

Surface of crystalline MNPs is also covered by hydroxyl groups and thus certain level of similarity can be shared with commonly studied amorphous silica filled PNCs. Both, PEG and ester groups can be found in the backbone of PEGDMA and bis-EMA molecules and polymer chains are expected to interact with a surface of MNPs in analogic attractive manner. Both monomers contain multiple reaction sites. The first one is ester group[91] bridging methyl methacrylate with PEG unit and each monomer molecule contains two ester groups at the ends of the molecule backbone. The second interaction site is situated on the oxygen in the backbone of PEG. These groups can act as Lewis acids coordinating their electron density with a hydrogen from surface HO– groups (Lewis base) and create hydrogen bonds. Bis-EMA monomer has a short PEG unit (n_{PEG}=1 and 2), on the other hand, PEGDMA monomer with n_{PEG}=16 can offer number of interaction sites. In addition, adsorption of initiator/initiating radicals on the surface of particles is not known.

If we will assume the existence of immobilised layer on the MNPs surface as well polymer chains bridging the contact between particles (however, could not be directly assessed by the analysis of the loss modulus and T_g), we will obtain hybrid polymer-Fe_3O_4 structures with a high inorganic content. It needs to be noted that

usually higher particle volume fractions are required to increase the fraction of bound polymer relative to that bulk chains in such extent that it is possible to macroscopically distinguish the signal from immobilized chains. Here, we are dealing with a particle loading ϕ=1 vol. % and a complication in the form of decreased photopolymerization yield. Despite this fact, changes induced by particle assemblies on mechanical properties are tremendous. Figure 5A shows an inner particle structure of the magnetic chain in sample B=25 mT from STEM observation.

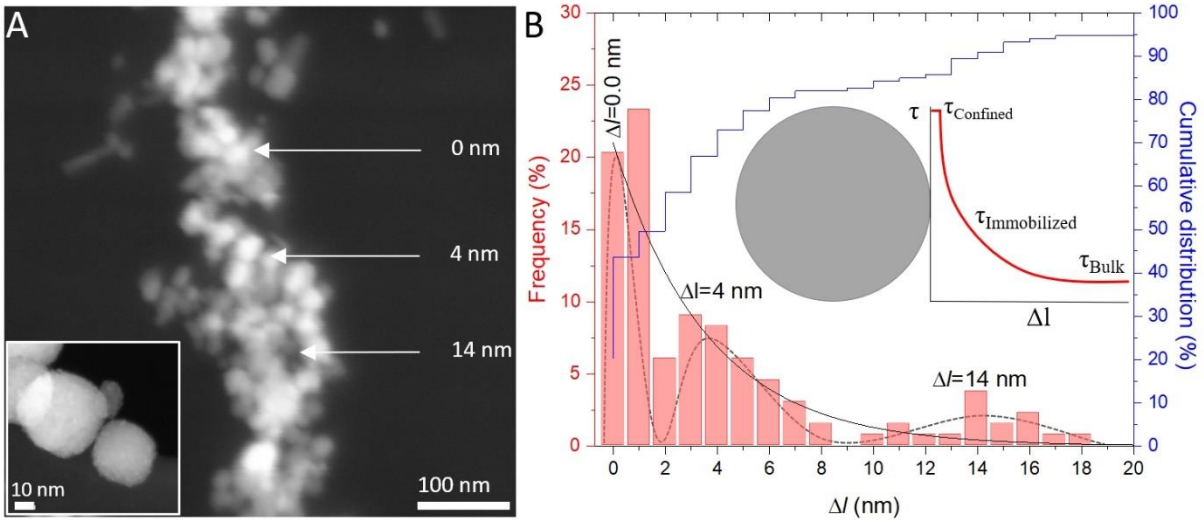

Figure 5 (A) STEM image of anisotropic structure assembled in B=25 mT after 10 seconds with ϕ=1 vol. % of particles in photopolymer matrix (dark areas is polymer). Arrows show typical places with a characteristic spacing. Dark field HR-TEM inset in (A) shows the most frequent situation when particles are in close contact resulting in $\Delta l \approx 0$ nm but their radius gives a rise to non-zero interparticle spacing suitable for polymer bridging. (B) Distribution of interparticle surface-to-surface distances Δl for the closest particle neighbors in the cluster from (A). Inset in (B) shows schematic depiction of relaxation time dependence on distance from particle surface.

Nanoparticles are spaced with a thin layer of polymer. Interparticle surface-to-surface distance between closest neighbours was measured and trimodal distribution is plotted in Figure 5B. Mostly, particles are in direct contacts or distanced within the sub nanometer range. The radius of particles gives an opportunity for polymer occupation of this space. The second distribution peak is around 4 nm and third one around 14 nm. Both are large enough to accommodate the polymer coils or monomers. Other assembling fields exhibit quite similar particle packing and thus structures are something between aggregate and clusters while this nature depends on actual position within particle chain. Interparticle distances are considerable short in magnetically concentrated assemblies and behaviour of such system can find analogy with highly filled PNCs[92-94] or even analogy with a structure of platelets in nacre and/or mineralized collagen fibrils in bone[95]. Polymerization degree of confined monomer units within the structures is not known. It will be assumed that monomers adsorbed on the particles and polymerized in confined space requires

minimum space approximately 2*R*g=2.4 nm to fit into the interparticle space without the change in chain conformation due to squeezing ($R_{g\ PEGDMA}$≈1.2 nm, approximated to $PEG_{Mw=1000}$[90], gyration radius of bis-EMA is expected to be lower and more anisotropic). In case of the shorter distances ($\Delta l < R_g$), monomer coil cannot occupy this space without further reduction of gyration radius[94, 96] or occupation of anisotropic shape[97] and consequently drastic modification of chain rigidity.

Various researchers claimed that strongly bound and confined polymer chains may behave as glass even at the temperatures when the bulk polymer is already completely unvitrified. This effect results in the vast increase of reptation/relaxation times, rubbery plateau, or fully disappeared terminal zone commonly evidenced in rheological measurements of highly filled PNCs melts. For example, Mujtaba et al.[98]measured the fraction of surface-immobilized polymer by NMR and detected significant fraction of segments with glassy relaxation times at temperatures of rubbery plateau of SBR/silica PNC. Fraction of glassy segments decreases with a temperature and it is dependent on particle volume fraction and level of confinement (caused by particle percolation). Similar NMR results were also published by Berriot et a.[99] and Chen et al.[93] also outlined that some segments might still appear as glassy in highly filled PNCs melts when interparticle distances are close or even lower than a length of Kuhn's segment. In these systems, unvitrified glass is preserved at particle loadings far above tens of volumetric percent.

Despite very low total fraction of MNPs in our systems, polymers shells are brought close enough to percolate due to magnetic interactions between particles or their assemblies during self- and magnetic assembly. Magnetic field increases local concentration of inorganic content considerably beyond the percolation threshold with a local particle volume fraction inside the particle chains calculated as ϕ_{local}~52 vol. %. This is close to maximum volume occupation for randomly packed spheres. Such short interparticle distances, vast enhancement of rubbery modulus and local particle volume fraction inside the magnetic chains indicate that there might be still a fraction of unvitrified polymer segments trapped inside the particle clusters. Term '*glassy*' will refer to polymer segments with retarded relaxations compared to bulk matrix, in our PNCs.

The percolation of glassy fraction of polymer and creating of continuous glassy backbone in soft matters (above T_g) is believed to be mainly responsible for the thermo-mechanical response of PNCs. Concept of percolated bridging glassy layer seems to be reasonable explanation for thermo-mechanical response of PNCs mainly due to its time-temperature dependence and viscoelastic appearance. Tauban et al. [100] modelled the mechanical response of PNCs with confined polymer chains within the particle structures of various morphologies and packings based on previous experimental results and theories[99, 101-103]. They present a plot of reinforcing ratio versus distance from T_g which exhibit very similar temperature dependence of reinforcing ratio for highly filled PNCs as plotted in Figure 4D for systems studied in this thesis. Such processing of thermo-mechanical data with a '*bell-like*' temperature dependence and maximum of reinforcing effectivity in transition region

is universal for all PNCs. Therefore, distance of PNCs from its *T*g and rubbery plateau is important to be specified in scientific texts dealing with a mechanical response of PNCs! Constant portion of storage modulus of PNCs at temperatures far above T_g is ascribed to deformation of bound glassy polymer with a significantly altered relaxation characteristic and stiffness high enough to avoid modulus drop.

Generally, particles assemblies in PNCs gradually form a nano, sub-micro, mirco and macroscopically percolated hybrid structures of various shapes and geometries with an increasing particle content. Consequently, nano, sub-micro, micro and macroscopic immobilized glassy polymer is formed in soft matrix[41, 42] and its shape and geometry are defined by particle arrangement. These hybrid structures can get under the deformation during the sample testing and exhibit non-zero stiffness. In our case, particles are organized in one-dimensional chains – fibers which may carry the load transferred from the matrix. To address orientation dependent mechanism of reinforcement by hybrid anisotropic structures, continuum micromechanics concepts will be employed. Micromechanics in combination with a model of composite with various structural motives was used to describe the mechanical response of biological hard tissues[104-106]. Complex reinforcing micro blocks commonly found in biological composites[95] were simplified by solid anisotropic microparticles arranged in polymer matrix in special geometrical patterns. Similar concept is used also here despite PNCs shows significant reinforcement only above T_g. Thus, such approximation and adopting of the micromechanical stress-transfer might not be relevant in whole temperature range, for studied PNCs. Hybrid micro chain structures of this work are approximated by solid fibres with a non-zero internal stiffness and homogeneous orientation. Depiction and description of model material with a multi-level hierarchy with images of individual levels of structure is depicted in Figure 6.

During the deformation of the composite, particle fibres are stretched. The stress is transmitted via bridging polymer within the structures and amount of stress carried by anisotropic hybrid structures dependent mainly on their orientation, length and their internal stiffness (E_F). Higher stiffness of hybrid structure than a stiffness of surrounding medium is essential requirement for the composite reinforcement ($E_F > E_M$). In opposite situation, structures will decrease the stiffness of composite. In longitudinal direction, larger portion of stress is transferred from low stiffness matrix while transversely oriented structures are less reinforcing effective [107]. Hence, transverse direction is comparable with self-assembled quasi-isotropic structures – similar volume of hybrid structures is locally under the deformation.

The internal stiffness of the hybrid structure (E_F) was calculated using semi-empirical Halpin-Tsai model[107]. This model is commonly used for prediction of the stiffness of polymers filled with micro fibers. Model was set to perfectly fit the experimental data by adjusting the stiffness of fibres (E_F). The stiffness of hybrid fiber in rubbery plateau is around $E_{F\ 150\,°C}$~400 MPa. This value is one order of magnitude higher than stiffness of the surrounding rubbery matrix. Temperature dependency of hybrid fiber structure stiffness is plotted in Figure 7A.

The stiffness of hybrid structure starts to rapidly increase from temperatures somewhere around 130-120 °C which is accompanied by the modulus upturn of its PNC. However, as vitrification of system proceeds the hybrid structure reach the maximum of its stiffness before reaching the T_g of the matrix. Stiffness of the hybrid structure seems to be constant and on the order of glassy matrix modulus far bellow T_g. Thus, it seems that structure was vitrified much earlier and at higher temperatures than surrounding matrix.

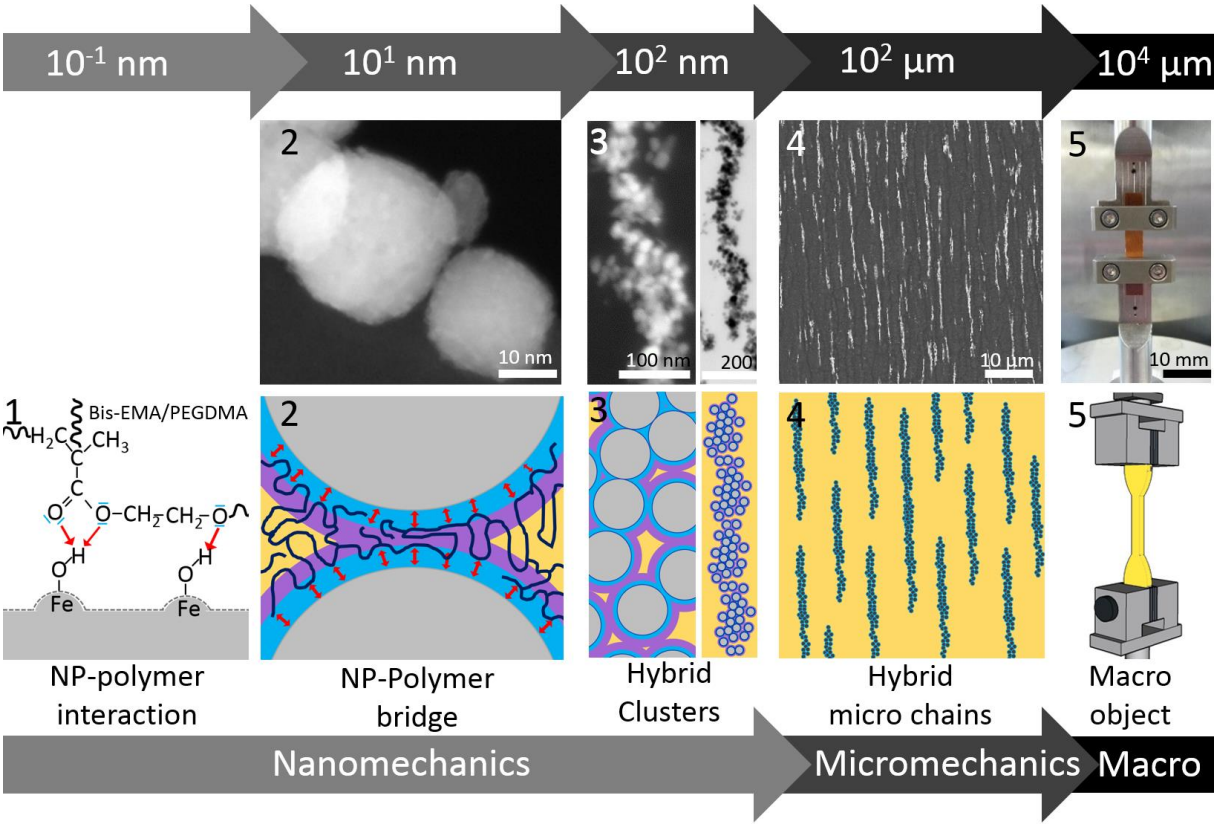

Figure 6 Model of magnetically assembled polymer nanocomposite with a multi-level hierarchy (bottom panel of the images) and the images of structural features at various levels (upper panel of the images). Arrows indicate a bottom-up formation of the material and the length scale of individual levels. Detailed description of the multi-level hierarchy is provided in following text bellow.

Continuum micromechanical interpretation of composite stiffness is only half of the mechanisms relying on load carrying capability of anisotropic structures and their stiffness which originates in nanoscopic interactions. More important question arise: *What causes the mechanical robustness of assemblie*? The finding of bridging laws between continuum macro/micromechanics and nanoscopic interactions might shed a light on the behaviour of complex nanostructures, biological structures and PNCs[34, 35]. For example, the extent of stress transfer into glass or carbon micro fibers depends on their length projected in tensile direction while their Young's modulus (E_F) is length independent and solely depends on the internal structure and stiffness of chemical bonds. The stiffness of hybrid structures is complex function of all nanoscopic mechanisms which contribute to nanoscopic deformations and hold the particle assemblies together such as: interparticle attractions (van der Waals,

electrostatic, magnetic, NP-NP interlocking, friction, etc.), deformation of particle atomistic structure, the strength of NP-polymer interactions and temperature dependent Young's modulus of polymer bridges[108-110].

Non-zero stiffness of NP-NP interaction might be an interesting concept, but stiffness of these interactions needs to be on the order of stiffness of surrounding medium to be reinforcing effective. It is assumed that stiffness of particle structure and strength of van der Waals attraction is frequency independent in common frequency ranges[88] and presumably also temperature independent (or much negligibly compared to polymers). Also, magnetic interactions are expected to become stronger with decreasing temperature and thus significantly contributes to PNC's stiffness at low temperatures. This makes interpretation of temperature dependency of reinforcing ratio via interparticle forces quite hard. And if these NP-NP interactions contribute to mechanical robustness of PNCs in some way, their effect will be strongest mainly in rubbery region. Despite, mechanical properties of particle aggregates exhibit some elastic features and non-zero stiffness[48-54], only stiffness of NP-NP bonds itself cannot explain the viscoelastic behaviour and disappearance of the reinforcement effect in PNCs close to their T_g. This feature is general for all PNCs using matrices of various mechanical properties. Same effect of the temperature on the reinforcement of PNCs is observed in this work. This means that forces which support the load carrying capability of the structures depend on the actual stiffness of surrounding medium and bound polymer layers and their vitrification characteristics.

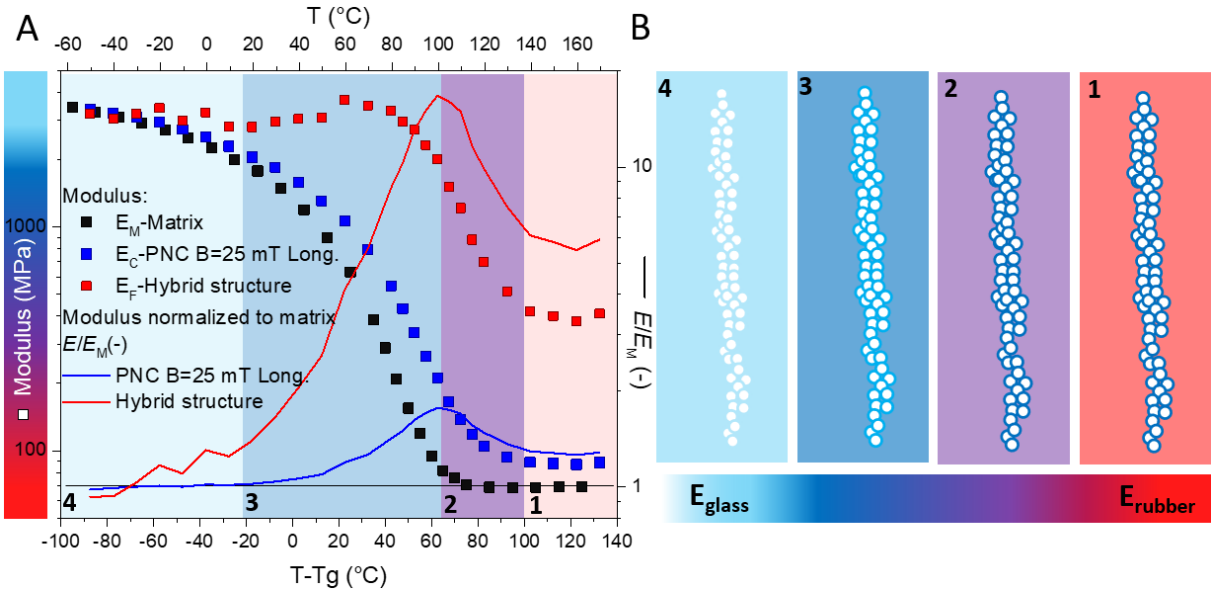

Figure 7 (A) Left *y*-axis – Dependency of calculated stiffness of hybrid structure (E_F) with modulus of neat matrix and PNC assembled in B=25 mT (square symbols □). Right *y*-axis – Relative ratio between stiffness of hybrid structure and its PNC normalized to matrix modulus (solid lines ─). (B) Schematic depiction of vitrification process from rubbery through transition to glassy region. Color bar indicates a stiffness of individual components – hybrid fibers and surrounding matrix. White color represents a stiffness of magnetite particles.

The contribution of bound layer and particle deformation is discussed further in text. Theory for orientation and temperature dependent reinforcement of magnetically structured PNCs from rubber to glass is schematically depicted in Figure 7B and described in following text. Author believes that this mechanism can be used for description of the temperature dependent reinforcing effectivity in PNCs by a slight modification depending on the geometry of the particle assemblies varying from system to system.

Region 1 – Rubber

Immobilized polymer segments bridge MNPs clusters also in rubbery state of bulk matrix and give a rise to the stiffness of micro- and macroscopically percolated hybrid nanostructures. The stiffness of hybrid structure calculated using micromechanical models fairly aggress with this idea. The value of hybrid structure is one order of magnitude higher than modulus of neat rubbery matrix, see Figure 7A. The stress from the matrix is carried by the hybrid structure, due to large mismatch of their moduli, $E_F > E_M$ with 6-times higher stiffness than matrix. Also, structure orientation and its length play a role, thus self-assembled and transversely oriented systems are far less successful in system reinforcement and consequently they exhibit only small reinforcing peak (Figure 4D) on contrary to longitudinal orientations.

Region 2 – Increase of reinforcing ratio

This region is relatively narrow however, the most intense reinforcement of PNC occurs mainly here. During cooling, storage modulus of PNC starts to upturn rapidly bellow ~140 °C while stiffness of matrix remains almost constant for longer period of temperatures, see Figure 7A. As temperature decreases, strongly adsorbed and confined polymer segments in the nearness of NPs vitrify as first and bound the whole hybrid structure by stiff polymer layer with a stiffness far exceeding the properties of bulk matrix which still remain in rubbery state ($E_F >> E_M$). At the end of this region, matrix's modulus starts to upturn as well, and it will slowly catch-up with a hybrid structure. In the addition to large mismatch between E_F and E_M, enhanced stiffness on the interface between bulky matrix and hybrid structure might be beneficial for loading the structures. With an increasing load, polymer bridges may experience much extensive strain amplification which may contribute to stiffness of structures as well.

Region 3 – Decrease of reinforcing ratio

In this region bulk matrix is progressively vitrified and its modulus catch-up with the hybrid structure. Matrix stiffness is gradually increasing and mismatch between E_F and E_M is slowly vanishing ($E_F > E_M$). As their ratio becomes smaller and smaller, micromechanical stress transfer is also more ineffective and less load is carried by hybrid structures. Hybrid structure reach its maximum vitrification degree at much higher temperatures when compared to neat matrix, see Figure 7A. Note that, maximum modulus of vitrified glassy structure is comparable with the modulus of

matrix modulus far bellow T_g, such as T=T_g-100 °C. From this point, only matrix vitrifies and slowly wipes off the mismatch between moduli.

Region 4 – Glass

Since hybrid structure is already vitrified, only bulk matrix vitrifies with a vanishing of mismatch between their moduli around glass transition. Both phases are thus more or less the same glass ($E_F \approx E_M$) and reinforcement of PNCs modulus by the addition of NPs can be described by deformation of atomistic structure of filler phase – volume replacement. Discrepancies and shifting of modulus along *y*-axis may be attributed to significant confinement, anisotropic coil shapes, or enormous physico-chemical cross-linking with NPs.

5 CONCLUSION

It has been shown that the controlling of assembling process by the strength of external field, particle volume fraction, viscosity of medium and assembling time leads to variety of magnetic structures. Self-assembled systems exhibit relatively large particle aggregates formed by complex bottom-up aggregation process. Calculations of van der Waals and magnetic attraction exhibit the regions where particles are close enough to be magnetically attracted across relatively large distances even in absence of the external magnetic field. The application of magnetic field of various strengths resulted in controlled structuring of magnetic material in polymer matrix into fractal-like aggregates with an anisotropy and percolation on micro length scales structured at lower fields or homogenously oriented anisotropic one-dimensional particle chains structured at higher fields. Structures assembled after longer assembling times gradually transform into large microscopic fibers.

Mechanical response of magnetically structured PNCs exhibits significant anisotropy for longitudinally and transversely oriented structures. On the other hand, reinforcement of polymer matrix was observed only above the glass transition of matrix which is classic signature of PNCs. Reinforcement effect exhibits significant temperature dependence with a maximum in the temperature region around T_g+60°C. Anisotropy of PNCs systems was described by the different load carrying capability which is higher for longitudinally oriented structures while transversely oriented structures contribute only negligibly to mechanical robustness on PNCs. Approximation of anisotropic particle structures by solid hybrid fibers with a non-zero stiffness was utilized in combination with a micromechanics of composite systems. Temperature dependent stiffness of hybrid structures was calculated using Halpin-Tsai model. The intrinsic stiffness of magnetically structures were attributed to vitrification of polymer segments in the vicinity and confined by MNPs which penetrate thorough the particle structures and transmit the stress. The presence of polymer bridge with sufficiently high molecular weight and stiffness is absolutely essential for the mechanical robustness of PNCs. Proposed theory of reinforcement can be generally applied for all PNCs creating nano-, submicro-, micro- and macro particle structures.

REFERENCES

1. J. B. Hooper and K. S. Schweizer, *Macromolecules*, 2005, **38**, 8858-8869.
2. P. Lepcio, F. Ondreas, K. Zarybnicka, M. Zboncak, O. Caha and J. Jancar, *Soft Matter*, 2018, **14**, 2094-2103.
3. L. He, M. Wang, J. Ge and Y. Yin, *Accounts of Chemical Research*, 2012, **45**, 1431-1440.
4. J. J. Weis, *J. Phys.-Condes. Matter*, 2003, **15**, S1471-S1495.
5. J. J. Weis, *Mol. Phys.*, 2005, **103**, 7-10.
6. J. Richardi, M. P. Pileni and J. J. Weis, *Physical Review E*, 2008, **77**, 9.
7. J. Richardi, M. P. Pileni and J. J. Weis, *Journal of Chemical Physics*, 2009, **130**, 6.
8. C. Salzemann, J. Richardi, I. Lisiecki, J. J. Weis and M. P. Pileni, *Physical Review Letters*, 2009, **102**, 4.
9. J. W. Swan, J. L. Bauer, Y. F. Liu and E. M. Furst, *Soft Matter*, 2014, **10**, 1102-1109.
10. A. P. Hynninen and M. Dijkstra, *Physical Review Letters*, 2005, **94**, 4.
11. L. Ye, T. Pearson, Y. Cordeau, O. T. Mefford and T. M. Crawford, *Scientific Reports*, 2016, **6**, 9.
12. J. J. Weis, *Mol. Phys.*, 1998, **93**, 361-364.
13. J. Richardi and J. J. Weis, *Journal of Chemical Physics*, 2011, **135**, 10.
14. J. Richardi and J. J. Weis, *Journal of Chemical Physics*, 2013, **138**, 4.
15. J. Jestin, F. Cousin, I. Dubois, C. Menager, R. Schweins, J. Oberdisse and F. Boue, *Advanced Materials*, 2008, **20**, 2533-+.
16. D. Fragouli, R. Buonsanti, G. Bertoni, C. Sangregorio, C. Innocenti, A. Falqui, D. Gatteschi, P. D. Cozzoli, A. Athanassiou and R. Cingolani, *Acs Nano*, 2010, **4**, 1873-1878.
17. A. S. Robbes, F. Cousin, F. Meneau, F. Dalmas, F. Boue and J. Jestin, *Macromolecules*, 2011, **44**, 8858-8865.
18. K. E. Roskov, J. E. Atkinson, L. M. Bronstein and R. J. Spontak, *Rsc Advances*, 2012, **2**, 4603-4607.
19. H. Y. Yuan, I. J. Zvonkina, A. M. Al-Enizi, A. A. Elzatahry, J. Pyun and A. Karim, *Acs Applied Materials & Interfaces*, 2017, **9**, 11290-11298.
20. Z. Rigbi and J. E. Mark, *Journal of Polymer Science Part B-Polymer Physics*, 1985, **23**, 1267-1269.
21. G. B. Sohoni and J. E. Mark, *Journal of Applied Polymer Science*, 1987, **34**, 2853-2859.
22. C. Bellan and G. Bossis, *International Journal of Modern Physics B*, 2002, **16**, 2447-2453.
23. F. Xu, C. A. M. Wu, V. Rengarajan, T. D. Finley, H. O. Keles, Y. R. Sung, B. Q. Li, U. A. Gurkan and U. Demirci, *Advanced Materials*, 2011, **23**, 4254-4260.

24. D. Lorenzo, D. Fragouli, G. Bertoni, C. Innocenti, G. C. Anyfantis, P. D. Cozzoli, R. Cingolani and A. Athanassiou, *Journal of Applied Physics*, 2012, **112**.
25. P. Song, Z. J. Peng, Y. L. Yue, H. Zhang, Z. Zhang and Y. C. Fan, *Express Polymer Letters*, 2013, **7**, 546-553.
26. P. J. Krommenhoek and J. B. Tracy, *Particle & Particle Systems Characterization*, 2013, **30**, 759-763.
27. S. R. Mishra, M. D. Dickey, O. D. Velev and J. B. Tracy, *Nanoscale*, 2016, **8**, 1309-1313.
28. S. Marchi, A. Casu, F. Bertora, A. Athanassiou and D. Fragouli, *Acs Applied Materials & Interfaces*, 2015, **7**, 19112-19118.
29. C. Hintze, D. Y. Borin, D. Ivaneyko, V. Toshchevikov, M. Saphiannikova-Grenzer and G. Heinrich, *Kgk-Kautschuk Gummi Kunststoffe*, 2014, **67**, 53-59.
30. D. Le Roy, D. Dhungana, L. Ourry, M. Faivre, R. Ferrigno, A. Tamion, V. Dupuis, V. Salles and A. L. Deman, *AIP Adv.*, 2016, **6**, 6.
31. J. P. Ge, H. Lee, L. He, J. Kim, Z. D. Lu, H. Kim, J. Goebl, S. Kwon and Y. D. Yin, *Journal of the American Chemical Society*, 2009, **131**, 15687-15694.
32. D. Fragouli, B. Torre, F. Villafiorita-Monteleone, A. Kostopoulou, G. Nanni, A. Falqui, A. Casu, A. Lappas, R. Cingolani and A. Athanassiou, *Acs Applied Materials & Interfaces*, 2013, **5**, 7253-7257.
33. C. Peters, O. Ergeneman, G. A. Sotiriou, H. Choi, B. J. Nelson and C. Hierold, *Acs Applied Materials & Interfaces*, 2015, **7**, 193-200.
34. J. Jancar, *Journal of Materials Science*, 2008, **43**, 6747-6757.
35. J. Jancar, J. F. Douglas, F. W. Starr, S. K. Kumar, P. Cassagnau, A. J. Lesser, S. S. Sternstein and M. J. Buehler, *Polymer*, 2010, **51**, 3321-3343.
36. J. Kalfus and J. Jancar, *Journal of Polymer Science Part B-Polymer Physics*, 2007, **45**, 1380-1388.
37. J. Kalfus and J. Jancar, *Polymer*, 2007, **48**, 3935-3937.
38. J. Kalfus and J. Jancar, *Polymer Composites*, 2007, **28**, 365-371.
39. J. Kalfus and J. Jancar, *Polymer Composites*, 2007, **28**, 743-747.
40. J. Jancar and L. Recman, *Polymer*, 2010, **51**, 3826-3828.
41. J. Jancar, R. S. Hoy, A. J. Lesser, E. Jancarova and J. Zidek, *Macromolecules*, 2013, **46**, 9409-9426.
42. J. Jancar, R. S. Hoy, E. Jancarova and J. Zidek, *Polymer*, 2015, **63**, 196-207.
43. N. Jouault, P. Vallat, F. Dalmas, S. Said, J. Jestin and F. Boue, *Macromolecules*, 2009, **42**, 2031-2040.
44. N. Jouault, F. Dalmas, F. Boue and J. Jestin, *Polymer*, 2012, **53**, 761-775.
45. J. F. Moll, P. Akcora, A. Rungta, S. S. Gong, R. H. Colby, B. C. Benicewicz and S. K. Kumar, *Macromolecules*, 2011, **44**, 7473-7477.
46. J. Oberdisse, *Soft Matter*, 2006, **2**, 29-36.
47. T. A. Witten, M. Rubinstein and R. H. Colby, *Journal De Physique Ii*, 1993, **3**, 367-383.

48. S. K. Friedlander, K. Ogawa and M. Ullmann, *Journal of Polymer Science Part B-Polymer Physics*, 2000, **38**, 2658-2665.
49. Y. J. Suh, S. V. Prikhodko and S. K. Friedlander, *Microsc. microanal.*, 2002, **8**, 497-501.
50. Y. J. Suh and S. K. Friedlander, *Journal of Applied Physics*, 2003, **93**, 3515-3523.
51. W. Z. Rong, A. E. Pelling, A. Ryan, J. K. Gimzewski and S. K. Friedlander, *Nano Letters*, 2004, **4**, 2287-2292.
52. R. Bandyopadhyaya, W. Z. Rong and S. K. Friedlander, *Chemistry of Materials*, 2004, **16**, 3147-3154.
53. A. Dalis and S. K. Friedlander, *Nanotechnology*, 2005, **16**, S626-S631.
54. W. Z. Rong, W. Q. Ding, L. Madler, R. S. Ruoff and S. K. Friedlander, *Nano Letters*, 2006, **6**, 2646-2655.
55. P. S. Antonel, G. Jorge, O. E. Perez, A. Butera, A. G. Leyva and R. M. Negri, *Journal of Applied Physics*, 2011, **110**, 8.
56. K. Keshoju and L. Sun, *Journal of Applied Physics*, 2009, **105**, 5.
57. T. Nardi, M. Sangermano, Y. Leterrier, P. Allia, P. Tiberto and J. A. E. Manson, *Polymer*, 2013, **54**, 4472-4479.
58. V. Melinte, T. Buruiana, A. Chibac, N. Lupu, M. Grigoras and E. C. Buruiana, *Chemical Engineering Journal*, 2015, **259**, 542-551.
59. Y. Lalatonne, J. Richardi and M. P. Pileni, *Nature Materials*, 2004, **3**, 121-125.
60. C. Xu, K. Ohno, V. Ladmiral and R. J. Composto, *Polymer*, 2008, **49**, 3568-3577.
61. A. S. Robbes, J. Jestin, F. Meneau, F. Dalmas, O. Sandre, J. Perez, F. Boue and F. Cousin, *Macromolecules*, 2010, **43**, 5785-5796.
62. Y. Jiao and P. Akcora, *Macromolecules*, 2012, **45**, 3463-3470.
63. S. Sierra-Bermudez, L. P. Maldonado-Camargo, F. Orange, M. J. F. Guinel and C. Rinaldi, *J. Magn. Magn. Mater.*, 2015, **378**, 64-72.
64. M. Ashjari, A. R. Mahdavian, N. G. Ebrahimi and Y. Mosleh, *J. Inorg. Organomet. Polym. Mater.*, 2010, **20**, 213-219.
65. B. Bharti, A. L. Fameau, M. Rubinstein and O. D. Velev, *Nature Materials*, 2015, **14**, 1104-+.
66. J. H. E. Promislow and A. P. Gast, *Langmuir*, 1996, **12**, 4095-4102.
67. S. A. Majetich and M. Sachan, *Journal of Physics D-Applied Physics*, 2006, **39**, R407-R422.
68. S. E. Kushnir, P. E. Kazin, L. A. Trusov and Y. D. Tretyakov, *Russian Chemical Reviews*, 2012, **81**, 560-570.
69. J. Zidek, J. Kucera and J. Jancar, *Cmc-Computers Materials & Continua*, 2011, **24**, 183-208.
70. J. Zidek, 2018.
71. Z. Varga, G. Filipcsei and M. Zrinyi, *Polymer*, 2006, **47**, 227-233.

72. J. L. Mietta, M. M. Ruiz, P. S. Antonel, O. E. Perez, A. Butera, G. Jorge and R. M. Negri, *Langmuir*, 2012, **28**, 6985-6996.
73. R. A. Landa, P. S. Antonel, M. M. Ruiz, O. E. Perez, A. Butera, G. Jorge, C. L. P. Oliveira and R. M. Negri, *Journal of Applied Physics*, 2013, **114**, 11.
74. Y. Han, W. Hong and L. A. E. Faidley, *Int. J. Solids Struct.*, 2013, **50**, 2281-2288.
75. K. Ikemura, K. Ichizawa, M. Yoshida, S. Ito and T. Endo, *Dent. Mater. J.*, 2008, **27**, 765-774.
76. Y. H. Song and Q. Zheng, *Progress in Materials Science*, 2016, **84**, 1-58.
77. K. W. Putz, M. J. Palmeri, R. B. Cohn, R. Andrews and L. C. Brinson, *Macromolecules*, 2008, **41**, 6752-6756.
78. Y. Zare and H. Garmabi, *Journal of Applied Polymer Science*, 2012, **123**, 2309-2319.
79. E. Guth, *Journal of Applied Physics*, 1945, **16**, 20-25.
80. H. M. Smallwood, *Journal of Applied Physics*, 1944, **15**, 758-766.
81. P. Sotta, P. A. Albouy, M. Abou Taha, D. R. Long, P. Grau, C. Fayolle and A. Papon, *Macromolecules*, 2017, **50**, 6314-6322.
82. J. Jancar, *Polymer Composites*, 2008, **29**, 1372-1377.
83. H. Mortazavian, C. J. Fennell and F. D. Blum, *Macromolecules*, 2016, **49**, 298-307.
84. N. Jouault, J. F. Moll, D. Meng, K. Windsor, S. Ramcharan, C. Kearney and S. K. Kumar, *Acs Macro Letters*, 2013, **2**, 371-374.
85. S. E. Harton, S. K. Kumar, H. C. Yang, T. Koga, K. Hicks, E. Lee, J. Mijovic, M. Liu, R. S. Vallery and D. W. Gidley, *Macromolecules*, 2010, **43**, 3415-3421.
86. S. W. Cheng, B. Carroll, W. Lu, F. Fan, J. M. Y. Carrillo, H. Martin, A. P. Holt, N. G. Kang, V. Bocharova, J. W. Mays, B. G. Sumpter, M. Dadmun and A. P. Sokolov, *Macromolecules*, 2017, **50**, 2397-2406.
87. C. Housmans, M. Sferrazza and S. Napolitano, *Macromolecules*, 2014, **47**, 3390-3393.
88. H. L. Xu, Y. H. Song, Q. X. Zhang and Q. Zheng, *Polymer*, 2018, **138**, 139-145.
89. S. Y. Kim and C. F. Zukoski, *Macromolecules*, 2013, **46**, 6634-6643.
90. B. J. Anderson and C. F. Zukoski, *Macromolecules*, 2008, **41**, 9326-9334.
91. H. Mortazavian, C. J. Fennell and F. D. Blum, *Macromolecules*, 2016, **49**, 4211-4219.
92. J. Moll and S. K. Kumar, *Macromolecules*, 2012, **45**, 1131-1135.
93. Q. Chen, S. S. Gong, J. Moll, D. Zhao, S. K. Kumar and R. H. Colby, *Acs Macro Letters*, 2015, **4**, 398-402.
94. A. N. Rissanou, H. Papananou, V. S. Petrakis, M. Doxastakis, K. S. Andrikopoulos, G. A. Voyiatzis, K. Chrissopoulou, V. Harmandaris and S. H. Anastasiadis, *Macromolecules*, 2017, **50**, 6273-6284.

95. U. G. K. Wegst, H. Bai, E. Saiz, A. P. Tomsia and R. O. Ritchie, *Nature Materials*, 2015, **14**, 23-36.
96. G. Chen, A. N. Li, H. X. Liu, S. Y. Huang, Z. Q. Zhang, W. Liu, C. Zha, B. Li and Z. Z. Wang, *Composite Structures*, 2018, **190**, 160-168.
97. J. S. Meth and S. R. Lustig, *Polymer*, 2010, **51**, 4259-4266.
98. A. Mujtaba, M. Keller, S. Ilisch, H. J. Radusch, M. Beiner, T. Thurn-Albrecht and K. Saalwachter, *Acs Macro Letters*, 2014, **3**, 481-485.
99. J. Berriot, H. Montes, F. Lequeux, D. Long and P. Sotta, *Macromolecules*, 2002, **35**, 9756-9762.
100. M. Tauban, J. Y. Delannoy, P. Sotta and D. R. Long, *Macromolecules*, 2017, **50**, 6369-6384.
101. J. Berriot, F. Lequeux, L. Monnerie, H. Montes, D. Long and P. Sotta, *J. Non-Cryst. Solids*, 2002, **307**, 719-724.
102. H. Montes, F. Lequeux and J. Berriot, *Macromolecules*, 2003, **36**, 8107-8118.
103. S. Merabia, P. Sotta and D. R. Long, *Macromolecules*, 2008, **41**, 8252-8266.
104. B. Bar-On and H. D. Wagner, *J. Struct. Biol.*, 2013, **183**, 149-164.
105. B. Bar-On and H. D. Wagner, *Acta Biomater.*, 2013, **9**, 8099-8109.
106. B. Bar-On and H. D. Wagner, *Mater. Sci. Eng. C-Mater. Biol. Appl.*, 2013, **33**, 603-607.
107. J. C. Halpin Affdl and J. L. Kardos, 1976, **16**, **344–352**.
108. R. Hentschke, J. Hager and N. W. Hojdis, *Journal of Applied Polymer Science*, 2014, **131**, 9.
109. J. Hager, R. Hentschke, N. W. Hojdis and H. A. Karimi-Varzaneh, *Macromolecules*, 2015, **48**, 9039-9049.
110. J. Meyer, R. Hentschke, J. Hager, N. W. Hojdis and H. A. Karimi-Varzaneh, *Macromolecules*, 2017, **50**, 6679-6689.

AUTHOR'S CV

Education

2014-2018 Doctoral studies – Advanced materials at Brno University of Technology, Central European Institute of Technology (CEITEC)

2011-2014 Master degree – Chemistry, technology and properties of materials at Brno University of Technology, Faculty of Chemistry

2009-2011 Bachelor degree – Chemistry, technology and properties of materials at Brno University of Technology, Faculty of Chemistry

PhD Internships

Technische Universtät Wien (Austria) – Institute of Materials Science and Technology – research group of prof. Jürgen Stampfl. July - September 2017.

Weizmann Institute of Science (Israel) – Department of Materials and Interfaces – research group of prof. Daniel H. Wagner. October - December 2017.

Work experience

2013-present Researcher and lab. technician – Central European Institute of Technology, Brno University of Technology

Responsibilities: synthesis of inorganic and nanoparticles, polymers and polymer nanocomposites; evaluation of physical properties of (nano)composites and their structural analysis; review of scientific and technical literature; writing of scientific papers and reports, presentations and project proposals

Operator of: SEM and STEM, LM and CLSM, Mechanical testing, DMA, Rheology, WAXD, EDS, FTIR, DSC, TGA, Magnetometry

ABSTRACT

Magnetically directed self-assembly in polymer nanocomposites is studied in this dissertation thesis. Structuring of the polymer nanocomposites by application of relatively weak external magnetic fields (B=0-50 mT) has been proven to be convenient method for the control of their nano- and microstructure. The effect of the field strength, particle loading, viscosity and assembling time on the resulted structure was studied in different systems such as photopolymer, polyurethane or colloidally dispersed magnetic nanoparticles in acetone with a small amount of dissolved polymer. Self-assembled structures – without application of the external magnetic field exhibit a multi-step aggregation into nanoparticle assemblies with a complex shape. By the calculation of interaction energies between the nanoparticles, magnetic interactions were attributed to be mainly responsible for the aggregation in self-assembled systems. With an increasing magnetic field, magnetic nanoparticles are rapidly arranged into high aspect ratio one-dimensional particle chains with a homogenous orientation in the bulk polymer matrix. After prolonged assembling time, the structures gradually grow from small submicro structures to large microscopic superstructures. This method exhibits large potential to be used for controlled creation of wide variety of structures in polymer nanocomposites suitable for technological applications and/or for fundamental studies. Magnetically structured polymer nanocomposites show significant directional anisotropy of composite's stiffness at the temperatures above glass transition of the system while there is no effect on the mechanical response in glassy state. Longitudinally oriented structures exhibit much stronger effect on the composite's stiffness. Reinforcing effectivity exhibits temperature dependent course with a maximum obtained approximately 60 °C above glass transition. The structure of magnetically assembled polymer nanocomposites was described by multi-level hierarchic model of material. Micromechanics was used to address the orientation dependent reinforcement and temperature dependent stiffness of the hybrid nanoparticle-polymer structures. Load carrying capability, deformation and non-zero stiffness of the hybrid structures were attributed to be responsible for the reinforcement of the polymer nanocomposites. The presence of polymer bridges between nanoparticles transmitting the stress through the magnetic structures is proposed to be essential for the mechanical properties of polymer nanocomposites and for stiffness of the hybrid structures.